The Astrophysical Journal, 668:806–814, 2007 October 20
© 2007. The American Astronomical Society. All rights reserved. Printed in U.S.A.

A DARK CORE IN ABELL 520[1]

Andisheh Mahdavi, Henk Hoekstra, Arif Babul, and David D. Balam
Department of Physics and Astronomy, University of Victoria, Victoria, BC V8W 3P6, Canada

and

Peter L. Capak
California Institute of Technology, MC 105-24, 1200 East California Boulevard, Pasadena, CA 91125
Received 2007 February 10; accepted 2007 June 18

ABSTRACT

The rich cluster Abell 520 ($z = 0.201$) exhibits truly extreme and puzzling multiwavelength characteristics. It may best be described as a "cosmic train wreck." It is a major merger showing abundant evidence for ram pressure stripping, with a clear offset in the gas distribution compared to the galaxies (as in the Bullet Cluster, 1E 0657−558). However, the most striking feature is a massive dark core (721 $h_{70}\ M_{\odot}/L_{\odot B}$) in our weak-lensing mass reconstruction. The core coincides with the central X-ray emission peak, but is largely devoid of galaxies. An unusually low mass-to-light ratio region lies 500 kpc to the east, and coincides with a shock feature visible in radio observations of the cluster. Although a displacement between the X-ray gas and the galaxy/dark matter distributions may be expected in a merger, a mass peak without galaxies cannot be easily explained within the current collisionless dark matter paradigm. Interestingly, the integrated gas mass fraction (≈0.15), mass-to-light ratio (220 $h_{70}\ M_{\odot}/L_{\odot B}$), and position on the X-ray luminosity–temperature and mass-temperature relations are unremarkable. Thus, gross properties and scaling relations are not always useful indicators of the dynamical state of clusters.

Subject headings: dark matter — galaxies: clusters: individual (Abell 520) — gravitational lensing — X-rays: galaxies: clusters

Online material: color figures

1. INTRODUCTION

Multiwavelength studies of galaxy clusters have revealed a richly textured intracluster environment, showing evidence of recent star formation in cluster cores and powerfully disruptive events such as active galactic nucleus (AGN) outbursts and mergers. Comparing observations of the hot intracluster medium and the weak gravitational lensing of distant sources has led to ever more precise constraints on the dark matter distribution in these systems (e.g., Miralda-Escude & Babul 1995; Allen et al. 2002; Dahle et al. 2003b; Smith et al. 2005; Mahdavi et al. 2007).

Of particular interest is the recent discovery of offsets between the dark matter distribution (as inferred from a weak-lensing mass reconstruction) and the hot gas distribution in X-ray emitting clusters. The Bullet Cluster (1E 0657−558) demonstrates the power of such a multiwavelength approach: a 4500 km s^{-1} cluster collision results in stripping of the gas from the dark matter halo of the smaller cluster, leaving a ≈100 kpc projected separation between the gas and lensing mass peaks (Markevitch et al. 2002; Clowe et al. 2004). This offset provides compelling geometrical evidence for the existence of dark matter (Clowe et al. 2006) as well as limits on the dark matter self-interaction cross section (Markevitch et al. 2004). Such mergers also offer an opportunity to study gas physics through direct comparison of the shock properties with the predictions of *N*-body and hydrodynamic simulations (Hayashi & White 2006; Springel & Farrar 2007).

These results suggest that studying *both* relaxed and merging clusters can yield significant insights into the nature of dark matter and the physics of the intracluster medium. With these goals in mind, we have recently begun the Canadian Cluster Comparison Project (CCCP),[2] a multiwavelength survey of 50 massive clusters with gas temperatures >5 keV, of which roughly half are dynamically disturbed.

During our survey we discovered that Abell 520 ($z = 0.201$; also known as MS 0451+02), a rich $10^{15}\ M_{\odot}$ merging system, exhibits truly extreme multiwavelength characteristics. In this paper we report on the results of a weak-lensing analysis and the subsequent comparison with the optical and X-ray properties of the cluster. The data are presented in § 2. In § 3 we describe the various mass constraints the data provide. In § 4 we discuss the implication for the cluster merger. The Appendix provides a detailed comparison of the weak-lensing results for the various data sets that were used. Throughout this paper we assume $H_0 = 70\ h_{70}$ km s^{-1} Mpc^{-1}, $\Omega_0 = 0.3$, and $\Omega_\Lambda = 0.7$.

2. DATA ANALYSIS

2.1. *Optical Imaging*

A major goal of the CCCP is the systematic study of the mass distribution of clusters using weak gravitational lensing. To this end we have obtained deep g' and r' wide field imaging data for a sample of 30 clusters with the Canada-France-Hawaii Telescope (CFHT) using MegaCam. The data for Abell 520 were obtained on 2004 November 13. The observations consist of four 400 s exposures in g' and eight 500 s exposures in r'. For our weak-lensing analysis we only consider the r' data because they are deeper and have better image quality.

The g' data are used to identify the cluster early type galaxies, using their location on the well-defined color-magnitude relation.

[1] Based on observations obtained with MegaPrime/MegaCam, a joint project of CFHT and CEA/DAPNIA, at the Canada-France-Hawaii Telescope (CFHT), which is operated by the National Research Council (NRC) of Canada, the Institute National des Sciences de l'Univers of the Centre National de la Recherche Scientifique of France, and the University of Hawaii.

[2] See http://www.astro.uvic.ca/~hoekstra/CCCP.html.

We select galaxies with $r < 22$ and $g' - r'$ colors up to 0.25 mag bluer than the redward edge of the red sequence, which enables us to map the cluster (red) light distribution and to compute the rest-frame B-band luminosity. By removing these galaxies from our weak-lensing catalogs, we also reduce contamination by cluster members (Hoekstra 2007).

The point spread function (PSF) introduces systematic changes in the shapes of the galaxies used in the weak-lensing analysis. Consequently correcting for the effects of the PSF is a critical part of our analysis. Current wide field imaging instruments such as MegaCam consist of a mosaic of chips, and special care needs to be taken to account for sudden jumps in the PSF properties when data from different exposures are combined. To avoid such problems altogether, the CCCP r' data are obtained in two sets of exposures. Each set of four 500 s exposures is taken with small dithers. The two sets are offset by approximately half a chip in each direction to fill in most of the gaps between chips. The image quality of the data is excellent with FWHMs of $0.50''$ and $0.57''$ as measured from the stacked sets. Each set is analyzed separately, which ensures that all data originate from the same chip. The resulting catalogs with shape parameters are then combined (see the Appendix for details).

Abell 520 has also been observed using Subaru with the Suprime-Cam in the i' and Cousins R_C bands. These data were used by Okabe & Umetsu (2007) in their weak-lensing analysis of the cluster. In order to compare to our CFHT observations, we retrieved these data from the Subaru archive and analyzed the data ourselves. The six R_C images were obtained on 2001 October 15 and 19 and have integration times of 300 s, with a seeing range from $0.52''$ to $0.65''$. The seven i' images were obtained on 2001 October 19 and November 17 and have integration times of 240 s. The image quality of these data is excellent as well, with the seeing ranging from $0.43''$ to $0.57''$.

The Subaru data were taken with relatively large offsets from exposure to exposure. Furthermore, the PSF showed large variations across the field of view and from image to image. We found that if we stacked the data, the resulting PSF pattern could not be corrected for to the level required for our analysis. Instead, we chose to analyze each exposure separately and to combine the weak-lensing shape catalogs. This approach significantly reduced residual systematics (to a negligible level).

2.2. *Weak-Lensing Shear Measurement*

Our weak-lensing analysis follows the procedures outlined in Hoekstra (2007) and is based on the algorithm described in Kaiser et al. (1995) with modifications described in Hoekstra et al. (1998, 2000). We refer the interested reader to those papers. We note that this implementation has been tested rigorously (e.g., Hoekstra et al. 1998; Heymans et al. 2006) and has been shown to be accurate at the few percent level. The first step in the analysis is the identification of the objects, which are subsequently analyzed. Our pipeline results in a catalog of ellipticities for the faint galaxies we use in our analysis. These shapes have been corrected for PSF anisotropy and the size of the PSF.

Figure 1 shows the resulting tangential distortion as a function of distance from the peak of the X-ray emission. To measure the signal we used the measurements obtained from the MegaCam r' data, selecting galaxies with $20 < r' < 25$. We detect a significant lensing signal, but as discussed below, the mass distribution in the central region is complicated, resulting in a decrease in the tangential distortion. To relate the observed lensing signal to an estimate of the mass requires an estimate of the mean source redshift distribution. To do so, we use the photometric redshift distribution from Ilbert et al. (2006), which is based on the CFHT

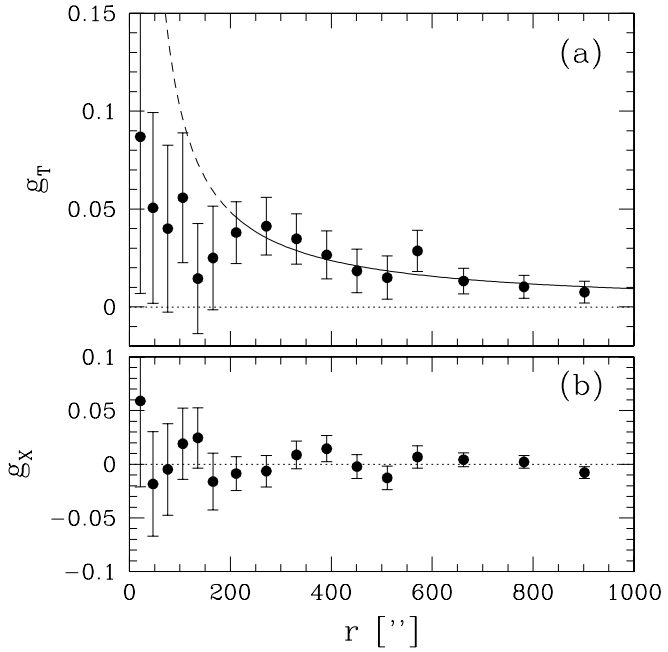

FIG. 1.—(*a*) Average tangential distortion as a function of distance from the peak of the X-ray emission using measurements from our MegaCam r' data ($20 < r' < 25$). The line is the best-fit singular isothermal sphere model, fitted to data at radii larger than $200''$; the corresponding velocity dispersion is 1028 ± 80 km s^{-1}. (*b*) Signal when the phase of the distortion is increased by $\pi/2$. If the signal observed in (*a*) is due to gravitational lensing, g_x should vanish, as is observed.

Legacy Survey Deep Fields. The strength of the lensing signal can be characterized by $\beta = \max[0, D_{ls}/D_s]$, where D_{ls} and D_s are the angular diameter distances between the lens and the source, and the observer and the source, respectively. We note that the value for β varies for the data sets considered here. In the Appendix we present a detailed comparison of the various catalogs, including an estimate for β for each. The selection of CFHT-detected objects used to compute the signal presented in Figure 1 results in $\beta = 0.60$. For reference, we fit a singular isothermal sphere model to the measurements at radii larger than $200''$ (Fig. 1, *solid line*). The best-fit velocity dispersion is $\sigma = 1028 \pm 80$ km s^{-1}.

For the surface density reconstruction use the direct inversion algorithm from Kaiser & Squires (1993), which works well for the wide field imaging data used here. The results are presented in Figure 2. We used the object catalog with all detected galaxies ($\beta = 0.59$) for this reconstruction and for all masses reported in the main text of the paper. The shape parameters of objects that were detected in multiple filters were averaged as discussed in the Appendix. Figure 2 also shows the optical, X-ray, and lensing maps for Abell 520. The resolution of the mass reconstruction is limited by the number density of source galaxies in these ground-based observations, and the FWHM of the Gaussian smoothing kernel is $\sim 60''$.

2.3. *Optical Spectroscopy*

Abell 520 was part of the Canadian Network for Observational Cosmology (CNOC) survey (Yee et al. 1996; Carlberg et al. 1996). Proust et al. (2000) independently measured redshifts for 29 galaxies within 1 Mpc of the X-ray center of Abell 520. We create a composite catalog by merging both redshift surveys; the detailed properties of this catalog will appear in a subsequent paper.

After a 3 σ clipping of the redshifts, we find a well-defined velocity peak with 71 member galaxies within 1 Mpc. The mean velocity is $cz = 60307 \pm 155$ km s^{-1}, or $z = 0.201$. The velocity dispersion within the same radius, corrected for $1 + z$ cosmological

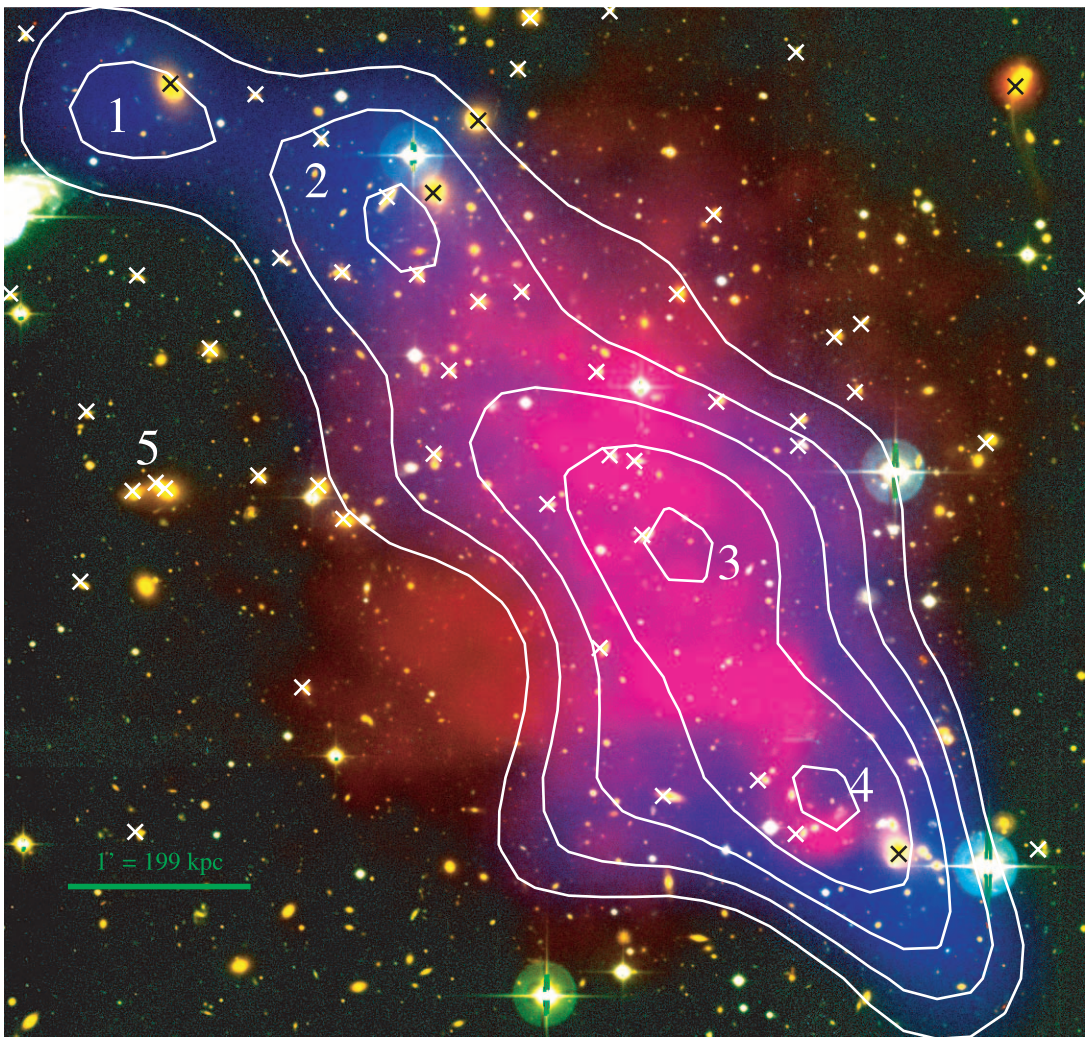

FIG. 2*a*

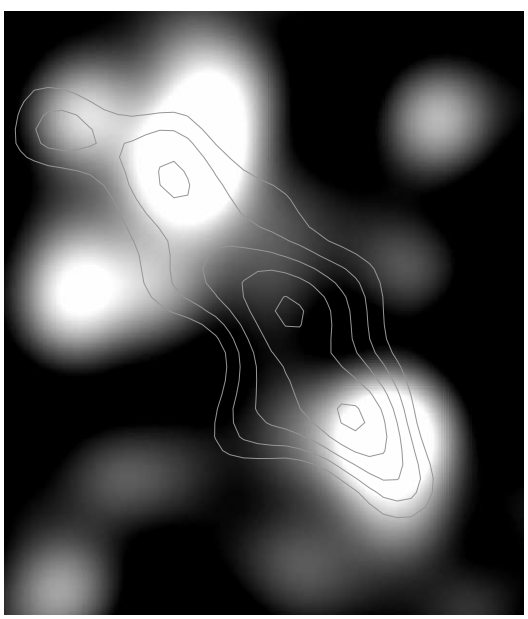

FIG. 2*b*

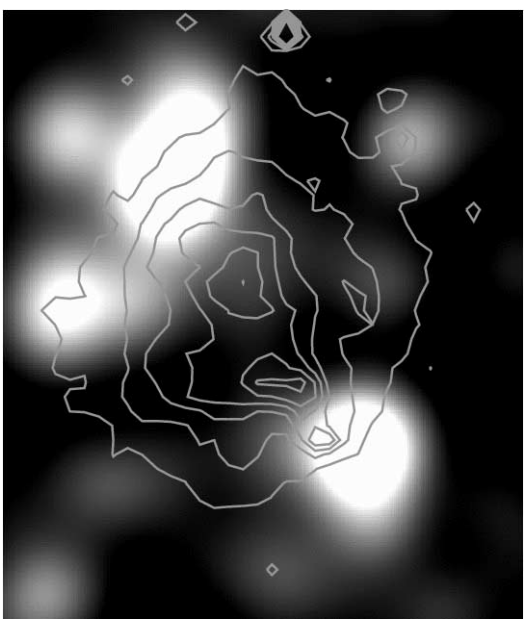

FIG. 2*c*

FIG. 2.—(*a*) Central $6.4' \times 6.4'$ of Abell 520, showing the CFHT image, the diffuse *Chandra* X-ray emission (*red*), and the lensing surface mass density (*blue*, + 3, 3.5, 4, 4.5, and 5 σ contours determined from a bootstrap analysis). Spectroscopically confirmed member galaxies are marked with crosses; red-sequence galaxies appear orange. (*b*) Red light distribution together with lensing contours from (*a*). (*c*) Same as (*b*), but with X-ray contours. Note the absence of galaxies in the central lensing peak. [*See the electronic edition of the Journal for a color version of this figure*.]

TABLE 1
X-Ray Properties of the Lensing Peaks

Peak	R.A. (J2000.0)	Decl. (J2000.0)	kT_X (keV)	Z_X ($Z_\odot$)	z	N_H (10^{22} cm^{-2})	Norm (10^{-18} cm^{-5})	L_X (10^{43} erg s^{-1})	l (Mpc)
1	04 54 19.94	+02 57 45.4	$8.0^{+2.4}_{-1.6}$	<2	0.201	0.018	$0.9^{+0.2}_{-0.3}$	0.5	1.1
2	04 54 14.08	+02 57 08.9	$13.5^{+3.4}_{-2.5}$	<0.31	0.201	0.018	$3.8^{+0.1}_{-0.2}$	1.8	1.6
3	04 54 10.41	+02 55 20.4	$9.8^{+0.7}_{-0.6}$	0.40 ± 0.10	0.201	0.018	11.0 ± 0.2	5.5	2.0
4	04 54 03.81	+02 53 30.3	$6.3^{+0.8}_{-0.6}$	$0.38^{+0.23}_{-0.22}$	0.201	0.018	$3.0^{+0.1}_{-0.2}$	1.5	1.7
5	04 54 20.05	+02 55 31.5	$10.7^{+2.8}_{-2.1}$	<2	0.201	0.018	$1.9^{+0.1}_{-0.2}$	1.0	1.7
Cluster	...	...	$9.3^{+0.4}_{-0.5}$	0.36 ± 0.05	0.209 ± 0.01	0.018 ± 0.005	75.5 ± 0.8	37.8	2.0

Notes.—Units of right ascension are hours, minutes, and seconds, and units of declination are degrees, arcminutes, and arcseconds. We list the position of each lensing peak, along with the best-fit MEKAL X-ray temperature and metallicity fit to data extracted within a 150 kpc radius circular aperture. "Cluster" is a circle centered on peak 3 with a 710 kpc radius. The redshift was fixed at the optical value, and the absorbing column was set to the best-fit value for the entire cluster. The plasma model normalization is $\int n_e n_H \, dV/4\pi D^2$, where n_e and n_H are the electron and proton space densities, and D is the comoving distance to the cluster. The X-ray luminosity is measured in the 0.5–2.0 keV band. The effective column along the line of sight for each peak, l, is conservatively estimated (see § 2). Errors are 1 σ; upper limits are at 90% confidence.

broadening, is 1120 ± 75 km s^{-1}. This value is in excellent agreement with the weak-lensing value of 1028 ± 80 km s^{-1}, based a singular isothermal sphere model fit to the signal.

2.4. *X-Ray Data*

We reanalyze ObsID 4215, the 67 ks *Chandra* X-ray observation originally described by Markevitch et al. (2005), using the CIAO version 3.3 reduction software and CALDB version 3.2.0 along with the standard background analysis tools.

We reapply the standard reduction pipeline, including the charge transfer inefficiency correction (Townsley et al. 2000), and calculate properly weighted response matrices using the CIAO `mkwarf` and `mkacisrmf` tasks. Point sources in the field are detected by the CIAO `wavdetect` package and masked. We use the CIAO blank sky fields to remove the particle background, and then subtract a $2' \times 2'$ area free of cluster emission to account for the cosmic and soft X-ray backgrounds. The X-ray center of the diffuse emission was taken to be the centroid of the cluster emission.

To analyze the spectra, we fit absorbed single-temperature MEKAL models. The X-ray measurements, including temperatures and luminosities, are shown in Table 1 and are consistent with the values reported by Markevitch et al. (2005) for the cluster.

Because of the complex, irregular mass distribution, spherical deprojection of the cluster to arrive at the gas mass is inappropriate. Instead, using the X-ray luminosity of the gas, we derive an upper limit on the gas mass *integrated within an aperture and along the line of sight*. Consider the Cauchy-Schwartz inequality

$$\left(\int \rho_g \, dV \right)^2 \leq \int \rho_g^2 \, dV \int dV, \qquad (1)$$

where ρ_g is the gas density and dV is the volume element along the line of sight. The left-hand side is the square of the gas mass, while the right-hand side is proportional to the X-ray luminosity times the emitting volume. To place an upper limit on the gas mass, one only requires an estimate of the column along the line of sight, l, which we take to be the value appropriate for a 1 Mpc radius sphere, $2(1 - d^2)^{1/2}$, where d is the projected distance of the extracted region from the X-ray center. This results in a generous upper limit because the visible extent of X-ray emission is only $\approx$600 kpc. Departures from sphericity can be accounted for in a straightforward manner: stretching the emitting column l by a factor of α gives a $\sqrt{\alpha}$ increase in the upper limit. We neglect departures from isothermality:[3] at the high temperatures reported here the luminosity varies only as $T^{1/2}$, and the gas mass upper limit would vary only as a $T^{1/4}$.

3. RESULTS

3.1. *Morphology*

Weak gravitational lensing studies of clusters allow us to reconstruct an "image" of the matter distribution that is independent of assumptions regarding the geometry or dynamical state of the cluster. This is a unique feature and crucial when studying complex systems such as Abell 520, as demonstrated here.

The striking incongruities in the stellar, gas, and dark matter distributions make this cluster a truly unique example of a massive, perhaps even multiple merger. The lensing map indicates that the cluster is aligned in the northeast-southwest direction, with four 5 σ peaks which we number 1–4. The northeast-southwest direction is corroborated by the *Chandra* data, which show an "arm" extending southwest from the main X-ray emitting region toward peak 4. The X-ray arm and accompanying shock were previously discussed by Markevitch et al. (2005). We also identify a fifth region (peak 5), with high red luminosity but low lensing mass. The properties of the five regions appear in Tables 1 and 2. The masses were determined directly from the lensing signal using a one-dimensional mass reconstruction (i.e., aperture mass densitometry; for details see Hoekstra 2007).

Peaks 3 and 5 are the most remarkable features of Abell 520 and deserve extended attention. The significance of peak 3 is comparable to the other mass peaks, yet its mass-to-light ratio is anomalously high, 721 $h_{70}\ M_\odot/L_{B\odot}$, compared to $\sim$200 for typical groups and clusters (Girardi et al. 2002). Conversely, peak 5 has a mass-to-light ratio that is strikingly low, $57 \pm 49\ h_{70}\ M_\odot/L_{\odot B}$. Furthermore, peak 5 also coincides with diffuse radio emission, as is readily apparent through a comparison of Figure 2*a* with Figure 1 of Markevitch et al. (2005). We discuss possible explanations for this remarkable configuration below (§ 4).

None of the three brightest cluster galaxies (BCGs; $M_B < -22$) are within peak 3; rather they are 690, 490, and 520 kpc from the center, located in peaks 1, 2, and 4, respectively. The brightest galaxy within 150 kpc of peak 3 has $M_B = -20.3$, hardly brighter than L^* at $z = 0.2$ (Croton et al. 2005; Dahlen et al. 2005). We know of no other groups or clusters without a $M_B < -20.3$ member within 300 kpc of coincident X-ray *and* lensing peaks.

3.2. *Reality of the Dark Peak*

Here we argue that peak 3 contains mostly dark matter and is physically associated with the cluster. First, the high $721\ h_{70}\ M_\odot/L_{\odot B}$ mass-to-light ratio argues for a deficit of stars

[3] The temperature dependence of the gas mass is negligibly affected by the free-free Gaunt factor g_{ff} (Rybicki & Lightman 1986).

TABLE 2
Masses and Mass-to-Light Ratios

Peak	M_{wl} ($h_{70}^{-1}10^{13}M_\odot$)	L_B ($h_{70}^{-2}10^{11}L_{\odot B}$)	Υ ($h_{70}M_\odot/L_{\odot B}$)	M_g ($h_{70}^{-2.5}10^{13}M_\odot$)	f_g ($h_{70}^{-1.5}$)
1	3.73 ± 0.99	1.59	234 ± 62	<0.12	<0.05
2	3.60 ± 1.04	4.22	85 ± 25	<0.28	<0.12
3	4.40 ± 1.09	0.61	721 ± 179	<0.52	<0.17
4	4.82 ± 0.89	3.56	135 ± 25	<0.25	<0.07
5	1.22 ± 1.06	2.13	57 ± 49	<0.22	<1
Cluster	49.98 ± 5.47	21.57	232 ± 25	<6.44	<0.15

Notes.—Shown are the projected lensing mass, the blue rest-frame luminosity, and the mass-to-light ratio for each lensing peak, measured within a 150 kpc aperture from the combined r', i', and R catalogs. "Cluster" is a circle centered on peak 3 with a 710 kpc radius. The parameters M_g, the cylindrical gas mass integrated along the line of sight within the same aperture, and f_g, the corresponding baryon fraction, are model independent (see § 2). Errors are 1 σ; upper limits are at 90% confidence.

in the peak. Second, the upper limit on the gas mass fraction, $f_g < 0.17$, suggests that ≳85% or 2.8×10^{13} $M_\odot$ of material has to be dark. If, for example, half the material within peak 3 were hot gas stripped from the plentiful reservoirs of the merger precursors, the observed X-ray luminosity would be ≈50 times greater than the measured 5.5×10^{43} erg s^{-1}.

Chance superpositions are a factor to be considered; a superposed background structure could mimic a dark peak. However, the multiwavelength data firmly rule out this hypothesis for a number of reasons. First, the X-ray spectrum of the gas exhibits the rest-frame 6.6 keV Fe line complex, which constrains the redshift of the X-ray emission within 1′ of peak 3 to be $z = 0.21 \pm 0.01$. Second, the brightest three galaxies in peak 3 all fall in the cluster red sequence and are spectroscopically verified cluster members according to the CNOC data. Finally, a background cluster along the line of sight would result in a detectable excess of galaxies at the position of the peak, which is not observed. The latter argument might be countered by considering a very high redshift ($z > 1$) cluster. However, the amplitude of the lensing signal and its dependence on limiting r' magnitude for the source galaxies clearly argue against such a high redshift.

A final source of concern is that peak 3 could arise from the superposition of two separate dark halos centered on peaks 2 and 4. If the two halos have recently passed through each other, the material in the overlapping portion could well give rise to a surface density enhancement. We estimate the amount of enhancement by approximating the matter distribution in peaks 2 and 4 as NFW (Navarro et al. 1997) spheres with density profiles $\rho_0(r/100\ \mathrm{kpc})^{-1}(1 + r/100\ \mathrm{kpc})^{-2}$, truncated at a distance of 2 Mpc from the X-ray center, with ρ_0 determined from the lensing data itself. We find that the total amount of mass within 150 kpc of peak 3 purely from the two intersecting NFW spheres is $\approx 2 \times 10^{12}$ $M_\odot$. This is an order of magnitude smaller than the dark mass implied by the X-ray and lensing observations. This result is insensitive to even large changes in the NFW concentration.

The available evidence therefore suggests that peak 3 is a distinct physical structure associated with Abell 520.

3.3. *Previous Studies*

Dahle et al. (2002) include Abell 520 in their weak-lensing study of 38 X-ray emitting clusters. They use the University of Hawaii 88 inch telescope with the 8K mosaic camera; the data have 0.9″ seeing, compared to 0.5″ for the Subaru and CFHT data. While the Dahle et al. (2002) map for Abell 520 does not recover all the features we see in our mass reconstruction, its most significant peak is centered very near (within 50 kpc) of our peak 3.

We note that our result differs from the analysis presented by Okabe & Umetsu (2007), also based on the Subaru data used here. They detect a significant mass at the position of peak 5, whereas peak 3 is not particularly pronounced. We believe that a problem with the PSF anisotropy correction is the source of the difference. Okabe & Umetsu (2007) analyzed the stacked data, which is problematic for the Abell 520 Subaru observations (see § 2.1).

To examine the robustness of the final surface density map, we also measured the weak gravitational lensing signal from the R, r', and i' data separately. We find that our results are robust, most notably the peak in the mass distribution that coincides with the peak of the X-ray emission (see the Appendix for more details regarding the comparison of the weak-lensing measurements).

4. INTERPRETATION

4.1. *Merger Characteristics*

The data suggest a head-on merger of roughly equal mass clusters along the northeast-southwest axis, with a possible secondary east-west merger related to peaks 3 and 5. Our interpretation is supported by the significant velocity structure associated with each of the mass peaks. The rest-frame line-of-sight velocities of the brightest galaxies in peaks 1, 2, 3, 4, and 5 are +67, −600, +700, +400, and −1300 km s^{-1}, respectively. The peaks are therefore clearly offset from each other in velocity space. Second, as is the case for the famous Bullet Cluster, 1E 0657−558 (Markevitch et al. 2002; Clowe et al. 2006), we find that the X-ray emission is offset from the galaxy distribution. This offset is expected for ram pressure stripping and is seen in gas + dark matter simulations of merging clusters (Poole et al. 2006). Furthermore, we observe low gas fractions in peaks 1 and 4 (Table 2). The postshock Mach number derived by Markevitch et al. (2005) for the peak 4 X-ray emission is ≈2.2, corresponding to a velocity of ≈1000 km s^{-1}. Combined with the peak 4 line-of-sight velocity, this suggests an inclination of ≈60° for the cluster and leads to a merging timescale of ≈1 Gyr.

Despite its extreme characteristics, Abell 520 would appear typical if its global integrated properties were considered alone (Tables 1 and 2). The integrated gas fraction, ≲0.15, is normal for clusters of this mass, as is its mass-to-light ratio, 220 $M_\odot/L_{\odot B}$ (Girardi et al. 2002).

The peak 3 mass-to-light ratio is larger than some previously published "extreme" values once they are corrected to our ΛCDM cosmology. For example, Gray et al. (2002) claim a 529 $M_\odot/L_{\odot B}$ for Abell 901b. What sets Abell 520 apart from previous work is the distinct lack of a BCG at the center of the dark peak. In the case of clusters such as Abell 901b, the dark matter peak and the

BCG are well aligned; but in Abell 520, all the bright galaxies are >400 kpc removed from the center of the dark peak. Abell 520 is unique because the lensing signal and the X-ray emission coincide in a region that lacks bright galaxies.

Remarkably, the cluster falls on the X-ray luminosity–temperature relation (Reiprich & Böhringer 2002; Lumb et al. 2004) and mass-temperature relation (Vikhlinin et al. 2006). Thus, while departures from scaling relations may be useful for gauging deviations from equilibrium, clusters consistent with these relations are not necessarily close to equilibrium or "preferred" in any other sense.

4.2. *Separating Dark from Light*

What truly distinguishes Abell 520 from other extreme clusters is the presence of a central dark region (peak 3) with almost no galaxies, and of a corresponding "light" region (peak 5) largely *devoid of dark matter*, i.e., consistent with being almost entirely baryonic based on both the X-ray and the optical data. Unlike the gas, both cold dark matter (CDM) and galaxies ought to be collisionless, and therefore even violent events should not be able to separate these two components. Having rejected the possibility of a background cluster, we now consider other possible explanations.

If we were to add all mass components of both peaks 3 and 5, we would have a peak with an ordinary mass-to-light ratio of 205 $h_{70}\ M_{\odot}/L_{B\odot}$ and baryon fraction <0.17. Given that the velocities of the galaxies in peak 5 are systematically blueshifted with respect to the cluster mean, it is highly likely that peak 5 is a dynamically distinct subsystem. Furthermore, peak 5 is coincident with both very hot X-ray emitting gas *and* diffuse radio emission, which together make a very strong argument for the existence of a secondary shock in the cluster. For these reasons we consider the possibility that peak 3 and 5 shared a common merger precursor, which passed through the cluster from the west to the east in projection on the sky.

The scenario most consistent with the CDM paradigm is that peak 3 occurred as a result of complex evolution during a multiple merger. Recent gas and dark matter simulations show that during such mergers, distortion and elongation of the original dark matter halos is commonplace (Poole et al. 2006). Recently, Sales et al. (2007) showed that under the right conditions, collapsed satellites falling in at late times could be ejected via three-body interactions after passing through the center of the host halo. Perhaps a similar process succeeded in ejecting the galaxies in peak 5 from their host halo, peak 3. It is unclear, however, whether the Sales et al. (2007) process could operate on a cluster scale, with galaxies embedded in a massive halo. We are currently conducting simulations to test this hypothesis.

A more intriguing possibility is that the dark matter concentration at the center of mass of the merger is due to the collisional deposition of dark matter. If the dark and light components (peaks 3 and 5) had a common origin, and the dark matter was collisionally stripped from this precursor, then Abell 520 is a counterexample to the Bullet Cluster. Markevitch et al. (2004) used the coincidence of the galaxy and lensing peaks in the Bullet Cluster to set an *upper* limit on the dark matter interaction cross section. For Abell 520, we use their equations (18)–(19) to estimate the necessary dark matter interaction cross section to produce peak 3.

Suppose that each of peaks 1, 2, 4, and 5 each contributed $\sim$25% of the total mass observed in the central dark peak. The chief unknown in the calculations is the surface density of each subcluster as viewed by an oncoming particle. For Abell 520, using the mass for peak 3 and assuming an effective depth along the merging axis of 150 kpc, we estimate $\Sigma_m \approx 0.066 \pm 0.016$ g cm^{-2}, yielding a cross section of $\sigma_{\rm dm}/m_{\rm dm} \approx 0.25/0.066 \approx 3.8 \pm 1.1$ cm^2 g^{-1}, well above the upper limit of 1 cm^2 g^{-1} derived for the Bullet Cluster. The depth could hardly be smaller than 150 kpc, and greater depths would only lead to higher cross sections. Other constraints from cluster mass profiles suggest $\sigma_{\rm dm} < 0.1$ cm^2 g^{-1} (Meneghetti et al. 2001; Dahle et al. 2003a; Arabadjis & Bautz 2005); these do not take the central baryon distribution into account. We note that light dark matter candidates such as axions and supersymmetric weakly interacting massive particles (WIMPs) have self-interaction cross sections many orders of magnitude below all the values discussed here (Kamionkowski 2002[4]).

The $\sigma_{\rm dm}$ value is an order-of-magnitude estimate, but any detailed corrections to the estimate must also be reflected in the upper limit derived for the Bullet Cluster. We caution that the measurement is sensitive to the surface density of the cluster along the merging direction, something that is uncertain in our current maps but will improve with planned higher resolution *Hubble Space Telescope* observations. Differences in the merger impact parameter could be invoked to explain why Abell 520 and the Bullet Cluster yield different constraints on the cross section; such a discussion is beyond the scope of this paper.

A final possibility is that we are observing a filament unrelated to the merger and by chance elongated almost exactly along the line of sight. The filament must be sparse enough that it fails to produce any significant galaxy concentration, sparse enough that it has little detectable X-ray emission, and long enough to produce the observed $4.4 \times 10^{13}\ M_{\odot}$ mass concentration. This hypothesis can be tested using our upcoming Sunyaev-Zel'dovich observations, which together with the X-ray data ought to reveal the structure of the gas along the line of sight.

5. CONCLUSIONS

The merging cluster Abell 520 demonstrates the power of multiwavelength techniques in revealing extreme phenomena in clusters of galaxies. Our study highlights the usefulness of studying unusual clusters. The most remarkable finding of this work is the evidence for a massive, 721 $h_{70}\ M_{\odot}/L_{\odot B}$ dark core that coincides with the peak in the X-ray emission, but is surprisingly devoid of bright galaxies. A "luminous" region containing little or no dark matter lies 500 kpc to the east.

To test the robustness of the weak-lensing analysis, we perform the first detailed study of multitelescope, multibandpass weak-lensing observations of clusters of galaxies. As shown in the Appendix, our joint analysis of the Subaru and CFHT data demonstrates that the dark peak in Abell 520 is not the result of instrumental effects, and that our methodology yields consistent results in the R, r', and i' bandpasses.

Using a model-independent analysis of the X-ray and optical data, we argue that the dark peak is physically associated with the cluster, and that it consists of $\gtrsim$85% dark matter. We estimate a timescale of 1 Gyr for the merger; together with the shock velocity derived by Markevitch et al. (2005), we derive an inclination of $\approx 60^{\circ}$ for the cluster.

Abell 520 lies on the cluster mass-temperature and luminosity-temperature relations. Therefore, consistency with cluster scaling relations is not necessarily an indicator that a cluster of galaxies is relaxed.

We consider possible mechanisms for separating the dark matter from the galaxies. Two possibilities stand out: (1) the galaxies originally in the dark core could have been ejected through a multiple-body interaction within the merging system; or (2) allowing for weakly self-interacting dark matter, the dark peak was deposited

[4] Audio presentation available at http://online.kitp.ucsb.edu/online/cmb02/kamionkowski/.

as a result of dark matter collisions during the merger impact; the required self-interaction cross section would be 3.8 ± 1.1 cm^2 g^{-1}. *N*-body simulations and higher resolution optical, X-ray, and radio data are required to distinguish among these and other possible explanations for this "cosmic train wreck."

We thank the referee for comments that significantly improved the paper. We are especially grateful to Howard Yee and Erica Ellingson for sharing the Abell 520 CNOC velocity data. We thank Maxim Markevitch, Mike Gladders, Neal Katz, Christoph Pfrommer, Pat Henry, Julianne Dalcanton, Kathleen Mahdavi, Gil Holder, and Greg Poole for insightful discussions. A. B. and H. H. acknowledge support from NSERC. A. B. also acknowledges support from the Leverhulme trust in the form of a visiting professorship at Oxford and Durham Universities. H. H. also acknowledges support from CFI, BCKDF, and CIfAR. Additional research funding was provided by J. Criswick.

APPENDIX

DETAILED COMPARISON OF CFHT AND SUBARU MULTICOLOR DATA

The combination of MegaCam r' data and Subaru R_C and i' data provides a unique opportunity to study the weak-lensing signal as a function of telescope and bandpass filter. Such a comparison is useful because it provides a test of our ability to remove observational distortions, which may be telescope or filter dependent. Below we demonstrate that our reduction procedure yields consistent mass reconstructions for all the instrument/filter combinations. In the case of Abell 520 this finding also strengthens our confidence in the detection of the "dark" peak 3.

There are a number of potential sources of systematics. One of these results from errors in astrometry. First, scale variations can lead to spurious shears. Second, when stacking data, the images need to be aligned well in order to avoid anisotropies in the galaxy shapes. For our analysis we first ensure that the images are aligned well. We compare the rms residuals in the positions of all nonsaturated pointlike sources within 15′ of the X-ray center. We find that the Subaru R and i' images have an rms deviation of 0.3 pixels, or 0.06″ (0.2 kpc) with respect to the CFHT image. Differences in the astrometric calibration are therefore negligible for the purposes of our comparison of the lensing signal.

As described in § 2.1 we measure the galaxy shapes from two independent sets of MegaCam r' data. Similarly, we obtain shape catalogs for each of the Subaru exposures (corrected for PSF anisotropy). The next step is to create a master catalog per bandpass by averaging the ellipticities of the galaxies that are found in multiple catalogs. Note, however, that for large (and bright) galaxies the error in the lensing signal is dominated by their intrinsic shape. Therefore, combining their shape measurements improves the weak-lensing measurements only slightly. However, the results do improve more for the faint galaxies, for which the measurements are dominated by noise in the image.

The previous step results in three master catalogs, one for each filter. We use this catalog to determine the aperture masses (Hoekstra 2007) for each of the five peaks shown in Figure 2. However, the various selections (e.g., magnitude cuts, accuracy in the shape measurement) result in different effective source redshift distributions. We used the photometric redshift distributions derived by Ilbert et al. (2006) to estimate β for each catalog. The resulting values are listed in Table 3.

The points in the top row of Figure 3 show the resulting aperture masses (150 kpc radius) for each filter and peak. The agreement between the estimates is excellent. Importantly, a significant amount of matter is detected around peak 3, whereas little signal is present at peak 5: we find the same result in both Subaru and CFHT data, which have very different systematics.

We also combine the three master catalogs into a single catalog which is used to produce the mass reconstruction in Figure 2 and mass estimates in Table 2. The masses obtained from this catalog are indicated by the shaded areas in the top row of Figure 3.

Instead of considering all detected galaxies, we can limit the analysis to galaxies detected in all three filters. In this case the intrinsic shapes of the sources are almost completely removed from the error budget. The resulting masses are shown in the bottom panel of Figure 3. As before the shaded area is the average of the three (matched) catalogs. As expected the variation from filter to filter is very small, with somewhat larger variation for peak 4. Note that in this case the value for β is almost filter independent (see Table 3).

Also in this case a significant mass is inferred for peak 3, whereas little mass is associated with peak 5. Of the above methods, the use of the unmatched catalog is the "traditional" approach, whereas the matched catalogs provide a strong test of instrument/bandpass cross calibration: in the absence of instrumental bias, use of the same exact galaxy catalog and technique ought to yield masses and mass reconstructions with highly correlated signal and noise.

TABLE 3
OBJECT SELECTION

Filter	Range (mag)	β		Mass Ratio				
		Unmatched	Matched	Cluster	Peak 1	Peak 2	Peak 3	Peak 4
r'	20–25	0.597	0.650	1.12 ± 0.19	1.03 ± 0.30	1.05 ± 0.45	0.89 ± 0.35	1.17 ± 0.34
R_C	20–25	0.578	0.659	1.07 ± 0.18	1.22 ± 0.39	0.99 ± 0.37	0.90 ± 0.34	0.78 ± 0.35
i'	22–25	0.648	0.660	1.02 ± 0.15	1.58 ± 0.66	1.84 ± 0.92	1.12 ± 0.41	1.02 ± 0.42
All	...	0.589	0.653	1.11 ± 0.17	1.50 ± 0.52	1.31 ± 0.50	0.99 ± 0.35	1.12 ± 0.41

NOTES.—Shown are the magnitude selection for the sources in the various filters, as well as the values for β for each selection. The table also lists the ratios of the inferred masses for the matched and unmatched catalogs. The value of β is computed using the photometric redshift distribution from Ilbert et al. (2006). The variation of β reflects the dependence on filter, but also includes the down-weighting of faint galaxies, for which shapes cannot be measured accurately.

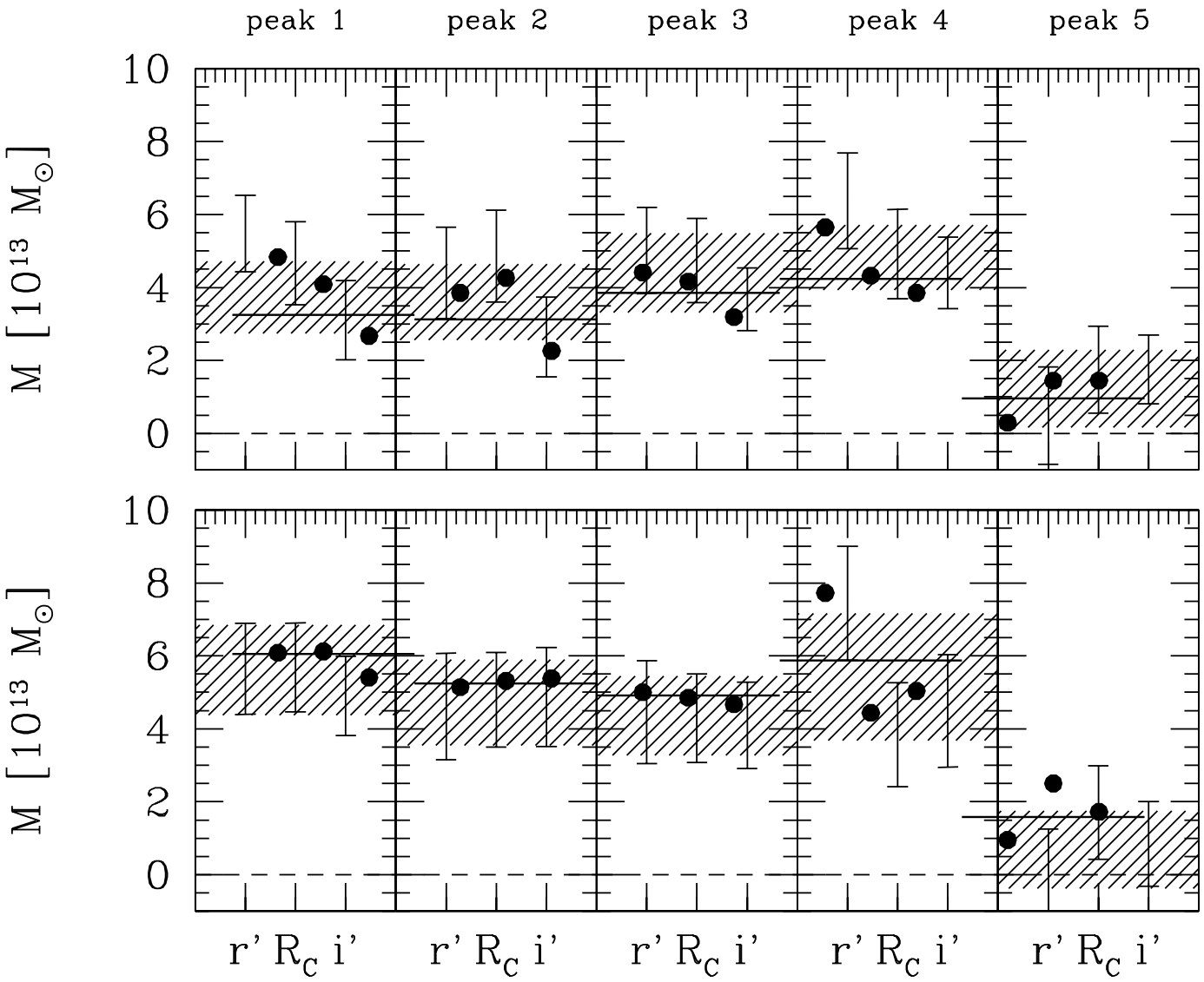

FIG. 3.— Comparison of aperture weak-lensing masses for all detected galaxies (*top row*) and only galaxies detected in all three images (*bottom row*). The shaded region shows the 1 σ error bar for the combined mass. The measured aperture masses are fully consistent across all filters and both instruments.

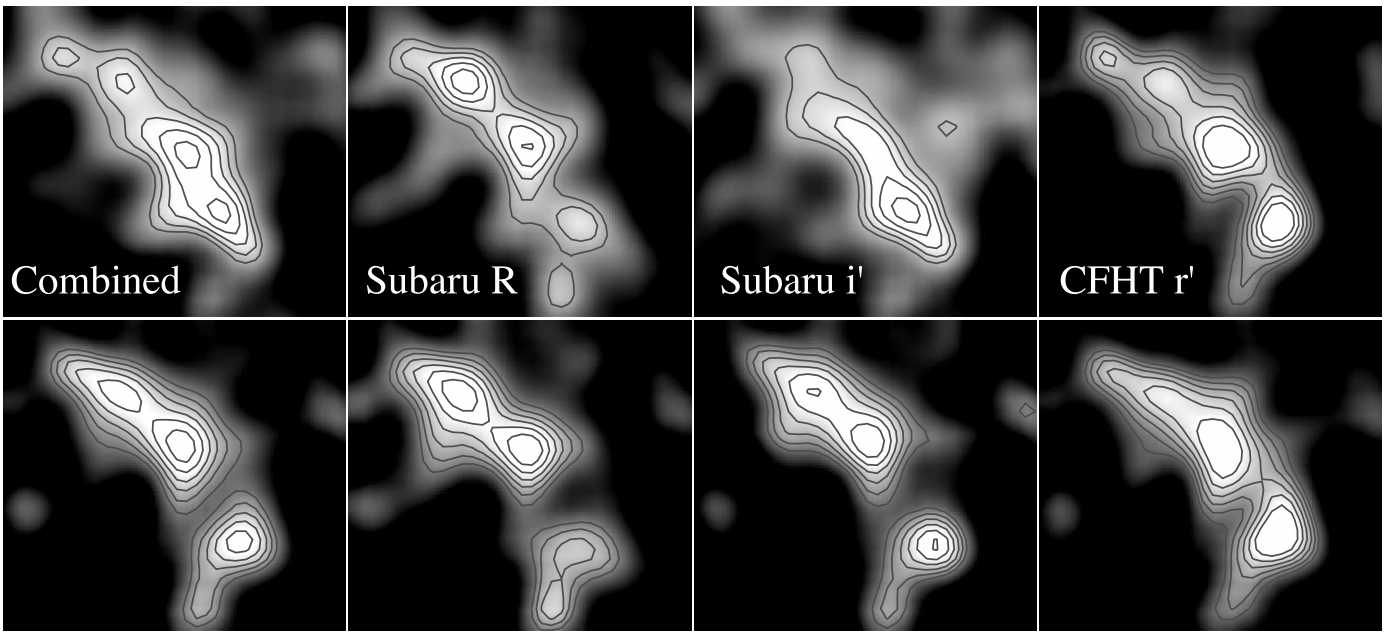

FIG. 4.— Surface mass reconstruction using all detected galaxies (*top row*) and using only galaxies detected in all three images (*bottom row*). Each column shows mass reconstructions using the Subaru R and i' and the CFHT MegaCam r' data; "combined" shows the mass reconstruction using all three colors. The contours show convergence levels equal to those in Fig. 1*a*. We recover the central dark peak in Abell 520 in all cases. [*See the electronic edition of the Journal for a color version of this figure.*]

We find that the masses obtained using the matched catalogs are somewhat higher compared to the unmatched catalogs. However, the ratios are consistent with unity within the errors. The ratios of the mass from the matched catalog to that of the unmatched sample for the various filters and peaks are listed in Table 3. We omit peak 5, because of its low mass, which leads to a meaningless ratio. The difference in mass between the two catalogs may well be caused by differences in the source redshift distributions which we did not account for. Nevertheless, this study demonstrates that we can recover the masses within $\sim$10% using different filters and telescopes.

Although the aperture mass estimates are of interest because of their easy interpretation, it is also useful to compare the actual surface mass density reconstructions. The results of the individual mass reconstructions are presented in Figure 4. The top row shows the results using the unmatched catalogs (r', R_C, i', and combined, from left to right), whereas the bottom row show the results for the matched catalogs.

The reconstructions are very similar, and the differences can be attributed to noise. Of particular importance for our work is the fact that we find that the dark peak (peak 3) is present in all data sets, regardless of whether we use only the matched galaxies or not; similarly, none of the reconstructions shows an overdensity at the position of peak 5.

These results differ from the Okabe & Umetsu (2007) reconstruction; they find a significant mass at the position of peak 5. We believe that a problem with the PSF anisotropy correction is a likely candidate, given the fact that Okabe & Umetsu (2007) analyzed stacked data. Based on our consistent results for both the CFHT and Subaru data, we are confident that the dark peak in Abell 520 is not the result of instrumental effects, and that our methodology yields consistent results in the R, r', and i' bandpasses.

REFERENCES

Allen, S. W., Schmidt, R. W., & Fabian, A. C. 2002, MNRAS, 334, L11
Arabadjis, J. S., & Bautz, M. W. 2005, Adv. Space Res., 36, 672
Carlberg, R. G., Yee, H. K. C., Ellingson, E., Abraham, R., Gravel, P., Morris, S., & Pritchet, C. J. 1996, ApJ, 462, 32
Clowe, D., Bradač, M., Gonzalez, A. H., Markevitch, M., Randall, S. W., Jones, C., & Zaritsky, D. 2006, ApJ, 648, L109
Clowe, D., Gonzalez, A., & Markevitch, M. 2004, ApJ, 604, 596
Croton, D. J., et al. 2005, MNRAS, 356, 1155
Dahle, H., Hannestad, S., & Sommer-Larsen, J. 2003a, ApJ, 588, L73
Dahle, H., Kaiser, N., Irgens, R. J., Lilje, P. B., & Maddox, S. J. 2002, ApJS, 139, 313
Dahle, H., Pedersen, K., Lilje, P. B., Maddox, S. J., & Kaiser, N. 2003b, ApJ, 591, 662
Dahlen, T., Mobasher, B., Somerville, R. S., Moustakas, L. A., Dickinson, M., Ferguson, H. C., & Giavalisco, M. 2005, ApJ, 631, 126
Girardi, M., Manzato, P., Mezzetti, M., Giuricin, G., & Limboz, F. 2002, ApJ, 569, 720
Gray, M. E., Taylor, A. N., Meisenheimer, K., Dye, S., Wolf, C., & Thommes, E. 2002, ApJ, 568, 141
Hayashi, E., & White, S. D. M. 2006, MNRAS, 370, L38
Heymans, C., et al. 2006, MNRAS, 368, 1323
Hoekstra, H. 2007, MNRAS, 379, 317
Hoekstra, H., Franx, M., & Kuijken, K. 2000, ApJ, 532, 88
Hoekstra, H., Franx, M., Kuijken, K., & Squires, G. 1998, ApJ, 504, 636
Ilbert, O., et al. 2006, A&A, 457, 841
Kaiser, N., & Squires, G. 1993, ApJ, 404, 441
Kaiser, N., Squires, G., & Broadhurst, T. 1995, ApJ, 449, 460
Kamionkowski, M. 2002, in The New Cosmology Confronts Observation: The Cosmic Microwave Background, Dark Matter, Dark Energy, and Brane Worlds, ed. K. Freese et al. (Santa Barbara: Kavli Inst. Theor. Phys.), http://online.kitp.ucsb.edu/online/cmb02/kamionkowski/
Lumb, D. H., et al. 2004, A&A, 420, 853
Mahdavi, A., Hoekstra, H., Babul, A., Sievers, J., Myers, S. T., & Henry, J. P. 2007, ApJ, 664, 162
Markevitch, M., Gonzalez, A. H., Clowe, D., Vikhlinin, A., Forman, W., Jones, C., Murray, S., & Tucker, W. 2004, ApJ, 606, 819
Markevitch, M., Gonzalez, A. H., David, L., Vikhlinin, A., Murray, S., Forman, W., Jones, C., & Tucker, W. 2002, ApJ, 567, L27
Markevitch, M., Govoni, F., Brunetti, G., & Jerius, D. 2005, ApJ, 627, 733
Meneghetti, M., Yoshida, N., Bartelmann, M., Moscardini, L., Springel, V., Tormen, G., & White, S. D. M. 2001, MNRAS, 325, 435
Miralda-Escude, J., & Babul, A. 1995, ApJ, 449, 18
Navarro, J. F., Frenk, C. S., & White, S. D. M. 1997, ApJ, 490, 493
Okabe, N., & Umetsu, K. 2007, PASJ, submitted (astro-ph/0702649)
Poole, G. B., Fardal, M. A., Babul, A., McCarthy, I. G., Quinn, T., & Wadsley, J. 2006, MNRAS, 373, 881
Proust, D., Cuevas, H., Capelato, H. V., Sodré, L., Jr., Tomé Lehodey, B., Le Fèvre, O., & Mazure, A. 2000, A&A, 355, 443
Reiprich, T. H., & Böhringer, H. 2002, ApJ, 567, 716
Rybicki, G. B., & Lightman, A. P. 1986, Radiative Processes in Astrophysics (New York: Wiley)
Sales, L. V., Navarro, J. F., Abadi, M. G., & Steinmetz, M. 2007, MNRAS, 379, 1475
Smith, G. P., Kneib, J.-P., Smail, I., Mazzotta, P., Ebeling, H., & Czoske, O. 2005, MNRAS, 359, 417
Springel, V., & Farrar, G. 2007, MNRAS, in press
Townsley, L. K., Broos, P. S., Garmire, G. P., & Nousek, J. A. 2000, ApJ, 534, L139
Vikhlinin, A., Kravtsov, A., Forman, W., Jones, C., Markevitch, M., Murray, S. S., & Van Speybroeck, L. 2006, ApJ, 640, 691
Yee, H. K. C., Ellingson, E., & Carlberg, R. G. 1996, ApJS, 102, 269